J|A|C|S ARTICLES

Published on Web 10/20/2009

Selective Characterization of Microsecond Motions in Proteins by NMR Relaxation

D. Flemming Hansen,*,† Haniqiao Feng,‡ Zheng Zhou,‡ Yawen Bai,‡ and Lewis E. Kay*,†

Departments of Molecular Genetics, Biochemistry, and Chemistry, The University of Toronto, Toronto, Ontario M5S 1A8, Canada, and Laboratory of Biochemistry and Molecular Biology, Center for Cancer Research, NCI, NIH, Bethesda, Maryland 20892

Received August 12, 2009; E-mail: flemming@pound.med.utoronto.ca; kay@pound.med.utoronto.ca

Abstract: The three-dimensional structures of macromolecules fluctuate over a wide range of time-scales. Separating the individual dynamic processes according to frequency is of importance in relating protein motions to biological function and stability. We present here a general NMR method for the specific characterization of microsecond motions at backbone positions in proteins even in the presence of other dynamics such as large-amplitude nanosecond motions and millisecond chemical exchange processes. The method is based on measurement of relaxation rates of four bilinear coherences and relies on the ability of strong continuous radio frequency fields to quench millisecond chemical exchange. The utility of the methodology is demonstrated and validated through two specific examples focusing on the thermostable proteins, ubiquitin and protein L, where it is found that small-amplitude microsecond dynamics are more pervasive than previously thought. Specifically, these motions are localized to α helices, loop regions, and regions along the rim of β sheets in both of the proteins examined. A third example focuses on a 28 kDa ternary complex of the chaperone Chz1 and the histones H2A.Z/H2B, where it is established that pervasive microsecond motions are localized to a region of the chaperone that is important for stabilizing the complex. It is further shown that these motions can be well separated from extensive millisecond dynamics that are also present and that derive from exchange of Chz1 between bound and free states. The methodology is straightforward to implement, and data recorded at only a single static magnetic field are required.

Introduction

Macromolecules such as proteins populate many microstates that differ in structure and energy. Molecular function is often dictated by the relative populations of these diverse states and their rates of interconversion, ranging from the nanosecond time-scale in the case of domain rearrangements to orders of magnitude slower for protein unfolding events.[1−4] Indeed, there is now increasing evidence to suggest that microsecond−millisecond (μs−ms) time-scale dynamics are used to navigate complex energy landscapes so as to connect various functional states.[5−7] A rigorous characterization of these dynamic processes is therefore a prerequisite for understanding protein function. Nuclear magnetic resonance (NMR) spectroscopy,[8,9] fluorescence spectroscopy (including fluorescence correlation spectroscopy),[10−13] and vibrational spectroscopy[14,15] have emerged as powerful techniques for characterizing the motions of macromolecules in solution. However, NMR spectroscopy is often the method of choice because site-specific dynamics information can be obtained at many positions throughout the molecule, often over a wide range of motional time-scales. Yet, it is precisely the sensitivity of the NMR method to this broad spectrum of time-scales that can make data analysis complex.

Consider the case of a protein tumbling in solution with an anisotropic diffusion tensor. Traditionally, backbone amide ^{15}N R_1, R_2, and steady-state ^{1}H−^{15}N NOE experiments[16] are

† The University of Toronto.
‡ Center for Cancer Research, NCI, NIH.

(1) Karplus, M.; Kuriyan, J. *Proc. Natl. Acad. Sci. U.S.A.* **2005**, *102*, 6679–6685.
(2) Lange, O. F.; Lakomek, N. A.; Farès, C.; Schröder, G. F.; Walter, K. F.; Becker, S.; Meiler, J.; Grubmüller, H.; Griesinger, C.; de Groot, B. L. *Science* **2008**, *320*, 1471–5.
(3) Yang, H.; Luo, G.; Karnchanaphanurach, P.; Louie, T. M.; Rech, I.; Cova, S.; Xun, L.; Xie, X. S. *Science* **2003**, *302*, 262–6.
(4) Vallurupalli, P.; Kay, L. E. *Proc. Natl. Acad. Sci. U.S.A.* **2006**, *103*, 11910–5.
(5) Boehr, D. D.; McElheny, D.; Dyson, H. J.; Wright, P. E. *Science* **2006**, *313*, 1638–42.
(6) Wolf-Watz, M.; Thai, V.; Henzler-Wildman, K.; Hadjipavlou, G.; Eisenmesser, E. Z.; Kern, D. *Nat. Struct. Mol. Biol.* **2004**, *11*, 945–9.
(7) Brueschweiler, S.; Schanda, P.; Kloiber, K.; Brutscher, B.; Kontaxis, G.; Konrat, R.; Tollinger, M. *J. Am. Chem. Soc.* **2009**, *131*, 3063–3068.
(8) Palmer, A. G.; Grey, M. J.; Wang, C. Y. *Methods Enzymol.* **2005**, *394*, 430–465.
(9) Palmer, A. G. *Curr. Opin. Struct. Biol.* **1997**, *7*, 732–737.
(10) Joo, C.; Balci, H.; Ishitsuka, Y.; Buranachai, C.; Ha, T. *Annu. Rev. Biochem.* **2008**, *77*, 51–76.
(11) Xu, J.; Knutson, J. R. *Methods Enzymol.* **2008**, *450*, 159–83.
(12) Gurunathan, K.; Levitus, M. *Prog. Nucleic Acid Res. Mol. Biol.* **2008**, *82*, 33–69.
(13) Xie, X. S. *J. Chem. Phys.* **2002**, *117*, p 11024–11032.
(14) Fayer, M. D. *Annu. Rev. Phys. Chem.* **2009**, *60*, 21–38.
(15) Kolano, C.; Helbing, J.; Kozinski, M.; Sander, W.; Hamm, P. *Nature* **2006**, *444*, 469–72.
(16) Kay, L. E.; Torchia, D. A.; Bax, A. *Biochemistry* **1989**, *28*, 8972–8979.

recorded, often at more than one static magnetic field strength, from which both site-specific internal "fast" dynamics (pico- to nanoseconds, ps−ns) parameters are extracted, as well as the principal components and orientation of the diffusion tensor. The obtained transverse relaxation rates are also sensitive to processes occurring on slower time-scales (μs−ms) that give rise to a contribution to R_2, R_{ex}, which is also fitted. In cases where μs−ms exchange is pervasive, such as for partially unfolded proteins, or even in certain regions of folded domains, it can be difficult to separate the different time-scale processes (ps−ns from μs−ms) in an accurate manner. Over the past decade, a number of NMR methods have been developed to address this issue. Original approaches were based on the measurement of ^{15}N, ^{1}H dipole−^{15}N chemical shift anisotropy cross-correlated relaxation interference[17−19] that is independent of chemical exchange. A more recent method, developed in our laboratory, measures the decay rates of four coherences, $R_2(2H_xN_z)$, $R_2(2H_zN_x)$, $R_2(2H_xN_x)$, $R_1(2H_zN_z)$ (see below), which can be combined in such a way so that contributions to relaxation from only pure dipolar interactions remain (that is, the effects of exchange are subtracted out). It is also possible, however, to take a separate linear combination of these four rates so that site-specific values for exchange contributions on the μs time-scale, $R_{ex,\mu s}$, are isolated, which forms the basis for the studies reported here.

There are a number of distinct advantages in using this (four-rate) approach to quantify exchange in proteins. First, the rates are already available as part of a larger study of ps−ns time-scale dynamics. Second, they can be recorded at only a single static magnetic field strength and with a single carrier offset. In contrast, other approaches such as those that extract exchange contributions from transverse relaxation rates are often based on measurements at multiple fields and assumptions about the time-scale of the chemical exchange process. Third, measurements such as off-resonance relaxation dispersion, which are complementary, require much longer measurement times because both the offset and the spin-lock field strength must be varied, with spin-lock field strengths that are significantly larger than the exchange process employed.

Herein, we establish the utility of this approach for measuring microsecond chemical exchange processes with a series of applications that quantify such dynamics in a pair of well-folded and thermally stabile proteins, human ubiquitin and the B1 immunoglobulin binding domain of peptostreptococcal protein L (protein L). We first cross-validate the methodology by comparing $R_{ex,\mu s}$ rates measured on these proteins using two different approaches, emphasizing that the new measurements eliminate the limitations of previous experiments that focus on extraction of exchange contributions from quantification of the magnetic field dependence of transverse relaxation rates. A major conclusion of the present study is that, despite the fact that both ubiquitin and protein L have been thought of in the past as rigid entities, with little dynamics of interest, the work here establishes that microsecond time-scale motions are present in α helices, loop regions, and in the rims of β sheets in both of these molecules, emphasizing that such dynamics are a likely feature of all proteins. In this regard, the results are consistent with elegant studies of Griesinger and co-workers based on residual dipolar coupling measurements in ubiquitin that make clear the importance of motion in the function of this protein.[2] A second application is presented involving the characterization of microsecond motions in the histone chaperone Chz1[20] in complex with the variant histone H2A.Z-H2B. We show that such dynamics can be separated from pervasive contributions to ^{15}N linewidths from millisecond time-scale motions that report on the association/dissociation process of the chaperone and from extensive nanosecond processes that vary significantly along the protein backbone.[21]

Results and Discussion

Isolation of Exchange Contributions. Molecular motions modulate the interactions between NMR active nuclei, leading to the relaxation of nuclear spins. Thus, accurate measurement of nuclear relaxation rates provides an avenue for probing molecular dynamics over a wide range of time-scales, from picoseconds to seconds. Micro- to millisecond time-scale chemical exchange processes (often referred to as "slow motions") enhance transverse nuclear relaxation rates, while motions with time-constants from picoseconds to nanoseconds ("fast motions") affect both longitudinal and transverse relaxation rates. A separation of different motional processes can be difficult in cases where large amplitude ps−ns and pervasive ms time-scale dynamics are present because contributions to the transverse relaxation rate from the slow motions (line broadening) and the fast motions (line narrowing) tend to cancel.

Previously, an approach for achieving this separation was described on the basis of recording four relaxation rates, corresponding to $R_2(2H_xN_z)$, $R_2(2H_zN_x)$, $R_2(2H_xN_x)$, and $R_1(2H_zN_z)$, where $R_{1,2}(2H_\nu N_\mu)$ is the autorelaxation rate of the coherence $2H_\nu N_\mu$ and H_ν and N_μ are the canonical Cartesian product operator density elements.[22] Two-dimensional NMR experiments for measuring these rates have been described in detail previously.[23] As described there, and below, the $R_2(2H_xN_z)$ rate is derived from the related rotating frame relaxation rate $R_{1\rho}(2H'_zN_z)$ that is measured in the presence of a continuous ^{1}H spin-lock radio frequency field, $R_2(2H_zN_x)$ follows from $R_{1\rho}(2H_zN'_z)$, while $R_2(2H_xN_x)$ is determined from $R_{1\rho^2}(2H'_zN'_z)$ that is measured in the presence of a double $\{^{1}H,^{15}N\}$ spin-lock. The individual autorelaxation rates[24−26] of the four relevant coherences above are given by

$$R_1(2H_zN_z) = \frac{d_{HN}^2}{8}(6J(\omega_N) + 6J(\omega_H)) + c_N^2 J(\omega_N) + \lambda_N + \lambda_H \quad (1)$$

(17) Kroenke, C. D.; Loria, J. P.; Lee, L. K.; Rance, M.; Palmer, A. G. *J. Am. Chem. Soc.* **1998**, *120*, 7905–7915.
(18) Ghose, R.; Huang, K.; Prestegard, J. H. *J. Magn. Reson.* **1998**, *135*, 487–99.
(19) Pelupessy, P.; Ferrage, F.; Bodenhausen, G. *J. Chem. Phys.* **2007**, *126*, 134508.
(20) Luk, E.; Vu, N. D.; Patteson, K.; Mizuguchi, G.; Wu, W. H.; Ranjan, A.; Backus, J.; Sen, S.; Lewis, M.; Bai, Y.; Wu, C. *Mol. Cell* **2007**, *25*, 357–68.
(21) Hansen, D. F.; Zhou, Z.; Fen, H.; Jenkins, L. M. M.; Bai, Y.; Kay, L. E. *J. Mol. Biol.* **2009**, *387*, 1–9.
(22) Sorensen, O. W.; Eich, G. W.; Levitt, M. H.; Bodenhausen, G.; Ernst, R. R. *Prog. Nucl. Magn. Reson. Spectrosc.* **1983**, *16*, 163–192.
(23) Hansen, D. F.; Yang, D.; Feng, H.; Zhou, Z.; Wiesner, S.; Bai, Y.; Kay, L. E. *J. Am. Chem. Soc.* **2007**, *129*, 11468–79.
(24) Abragam, A. *Principles of Nuclear Magnetism*; Clerendon Press: Oxford, 1961.
(25) Peng, J. W.; Wagner, G. *J. Magn. Reson.* **1992**, *98*, 308–332.
(26) Allard, P.; Helgstrand, M.; Hard, T. *J. Magn. Reson.* **1998**, *134*, 7–16.

$$R_2(2H_xN_z) = \frac{d_{HN}^2}{8}(4J(0) + J(\omega_H - \omega_N) + 3J(\omega_H) + 6J(\omega_H + \omega_N)) + c_N^2 J(\omega_N) + \vartheta_H + \lambda_N + R_{ex,\rho}(H_x) \quad (2)$$

$$R_2(2H_zN_x) = \frac{d_{HN}^2}{8}(4J(0) + J(\omega_H - \omega_N) + 3J(\omega_N) + 6J(\omega_H + \omega_N)) + \frac{c_N^2}{6}(4J(0) + 3J(\omega_N)) + \vartheta_N + \lambda_H + R_{ex,\rho}(N_x) \quad (3)$$

$$R_2(2H_xN_x) = \frac{d_{HN}^2}{8}(3J(\omega_N) + J(\omega_H - \omega_N) + 3J(\omega_H) + 6J(\omega_H + \omega_N)) + \frac{c_N^2}{6}(4J(0) + 3J(\omega_N)) + \vartheta_H + \vartheta_N + R_{ex,\rho}(2H_xN_x) \quad (4)$$

where $d_{HN} = (\mu_0/4\pi)\hbar\gamma_H\gamma_N r_{HN}^{-3}$, $c_N = B_0\gamma_N\Delta\sigma_N\sqrt{((1 + \eta_N^2/3)/3)}$, μ_0 is the permeability of free space, $\hbar$ is Planck's constant divided by 2π, γ_H and γ_N are the magnetogyric ratios of ^{1}H and ^{15}N, respectively, r_{HN} is the vibrationally averaged distance between ^{1}H and ^{15}N nuclei, B_0 is the static magnetic field strength, $\Delta\sigma_N = \sigma_{11,N} - (\sigma_{22,N} + \sigma_{33,N})/2$ (shift anisotropy), and $\eta_N = (\sigma_{22,N} - \sigma_{33,N})/(\sigma_{11,N} - \sigma_{iso,N})$ (reduced asymmetry), where $\sigma_{11,N}$, $\sigma_{22,N}$, and $\sigma_{33,N}$ are the principal components of the nitrogen CSA tensor[24,27] and $\sigma_{iso,N} = 1/3(\sigma_{11,N} + \sigma_{22,N} + \sigma_{33,N})$. The power spectral density function, $J(\omega)$, describes the frequency distribution of the stochastic motions that modulate both the ^{1}H$-^{15}$N dipole$-$dipole and the ^{15}N CSA interactions and in its simplest form is given by[28,29]

$$J(\omega) = \frac{2}{5}\frac{S^2\tau_C}{1 + \omega^2\tau_C^2} + \frac{2}{5}\frac{(1 - S^2)\tau'_e}{1 + \omega^2\tau'^2_e}, 1/\tau'_e = 1/\tau_C + 1/\tau_e \quad (5)$$

where S is an order parameter describing the amplitude of ps$-$ns motions occurring on the time-scale τ_e, and τ_C is the correlation time for the assumed isotropic motion. In what follows, the specific form of $J(\omega)$ is arbitrary, that is, the dynamics could be more complex than what is "captured" by eq 5; this has no effect on the robustness of the extracted exchange contributions because the only assumption about the spectral density function made below is that $J(\omega) \propto 1/\omega^2$ for $\omega > \omega_H + \omega_N$.[30,31] The contributions to the longitudinal relaxation of the ^{1}H (^{15}N) spin from interactions with external spins are given by λ_H (λ_N), while ϑ_H and ϑ_N are additions to ^{1}H and ^{15}N transverse relaxation rates, respectively, that result from interactions with proximal external spins and from other magnetization leaking mechanisms, such as exchange with the solvent. Finally, $R_{ex,\rho}(H_x)$ and $R_{ex,\rho}(N_x)$ are contributions to the $R_2(2H_xN_z)$ and $R_2(2H_zN_x)$ relaxation rates, respectively, which originate from chemical exchange processes that are measured in the presence of ^{1}H and ^{15}N spin-lock fields (see above). The corresponding contribution to the rate $R_{ex,\rho}(2H_xN_x)$ can be written to very good approximation as $R_{ex,\rho}(H_x) + R_{ex,\rho}(N_x)$ that follows directly from the fact that relaxation rates are measured under spin-locking conditions (see Supporting Information). In eqs 1$-$4, we have neglected contributions to relaxation from ^{1}H CSA; however, these subtract out in what follows below.

Previously, we showed that it is possible to isolate a pure dipole$-$dipole "chemical exchange-free" measure of ^{15}N backbone transverse relaxation, R_{dd}:

$$R_{dd} = (1/2)[R_2(2H_xN_z) + R_2(2H_zN_x) - R_2(2H_xN_x) - R_1(2H_zN_z)] \quad (6)$$

with small systematic errors due to cross-relaxation between amide protons and proximal proton spins minimized by recording spectra on proteins with deuteration levels of 50% or higher. We now turn our attention to quantification of the chemical exchange contribution to nitrogen transverse relaxation, $R_{ex,\rho}(N_x)$, that reports on micro-millisecond time-scale motions in proteins.[32$-$34] A linear combination of eqs 1$-$4 is constructed that isolates $R_{ex,\rho}(N_x)$ according to (see Supporting Information):

$$R_{ex,\rho}(N_x) + \vartheta_N = \frac{1}{2}\left\{R_1(2H_zN_z)\left(-1 + \frac{4c_N^2}{3d_{HN}^2}\right) + R_2(2H_zN_x) \times \left(1 - \frac{4c_N^2}{3d_{HN}^2}\right) + R_2(2H_xN_z)\left(-1 - \frac{4c_N^2}{3d_{HN}^2}\right) + R_2(2H_xN_x) \times \left(1 + \frac{4c_N^2}{3d_{HN}^2}\right)\right\} + \lambda_N - 0.035(3d_{HN}^2 - 4c_N^2)J(0.87\omega_H) \quad (7)$$

with each of the terms defined above and where the high frequency spectral density elements, $J(\omega_H + \omega_N)$, $J(\omega_H)$, and $J(\omega_H - \omega_N)$, have been combined using the relation $J(\varepsilon\omega) \approx (0.87/\varepsilon)^2 J(0.87\omega_H)$.[17,25,30] For macromolecules, $0.035(3d_{HN}^2 - 4c_N^2)J(0.87\omega_H)$ and λ_N can be neglected; for example, in the case of ubiquitin at 298 K, for which $\tau_C \approx 5$ ns (278 K; $\tau_C \approx 9$ ns), $0.035(3d_{HN}^2 - 4c_N^2)J(0.87\omega_H) = 1.6 \times 10^{-3}\ s^{-1} \pm 7 \times 10^{-4}\ s^{-1}$ ($9 \times 10^{-4}\ s^{-1} \pm 5 \times 10^{-4}\ s^{-1}$) on average, and this term will only get smaller with proteins of increasing size. Contributions to transverse relaxation of ^{15}N from external spins ϑ_N can be minimized by using highly deuterated samples (discussed previously in the context of measuring R_{dd}).[23] From the X-ray structure of protein L and using a value of $S^2 = 0.85$ for all ^{15}N-distal proton interactions, a maximum value of $\vartheta_N = 0.05$ (0.1) s^{-1} is calculated at 298 (278 K), assuming that the protein is deuterated at all positions other than amides, well below the accuracy of measurement of μs exchange contributions (see Supporting Information). In principle, ϑ_N can be separated from $R_{ex,\rho}(N_x)$ if measurements are carried out at multiple static magnetic fields and if the field dependencies of the individual contributions are known and are different. For example, for both ubiquitin and protein L considered here, $R_{ex,\rho}(N_x) \propto B_0^2$ (see below), while remote dipolar contributions are field independent. In what follows, we have assumed $\vartheta_N = 0$.

From the above discussion, it follows that to excellent approximation:

(27) Cornilescu, G.; Bax, A. *J. Am. Chem. Soc.* **2000**, *122*, 10143–10154.
(28) Lipari, G.; Szabo, A. *J. Am. Chem. Soc.* **1982**, *104*, 4546–4559.
(29) Lipari, G.; Szabo, A. *J. Am. Chem. Soc.* **1982**, *104*, 4559–4570.
(30) Farrow, N. A.; Zhang, O.; Szabo, A.; Torchia, D. A.; Kay, L. E. *J. Biomol. NMR* **1995**, *6*, 153–162.
(31) Ishima, R.; Nagayama, K. *J. Magn. Reson., Ser. B* **1995**, *108*, 73–76.
(32) Wang, L.; Pang, Y.; Holder, T.; Brender, J. R.; Kurochkin, A. V.; Zuiderweg, E. R. *Proc. Natl. Acad. Sci. U.S.A.* **2001**, *98*, 7684–9.
(33) Evenäs, J.; Malmendal, A.; Akke, M. *Structure* **2001**, *9*, 185–95.
(34) Akke, M. *Curr. Opin. Struct. Biol.* **2002**, *12*, 642–7.

$$R_{\mathrm{ex},\rho}(\mathrm{N}_x) = \frac{1}{2}\Bigg\{R_1(2\mathrm{H}_z\mathrm{N}_z)\left(-1 + \frac{4c_\mathrm{N}^2}{3d_\mathrm{HN}^2}\right) + R_2(2\mathrm{H}_z\mathrm{N}_x)\left(1 - \frac{4c_\mathrm{N}^2}{3d_\mathrm{HN}^2}\right) + R_2(2\mathrm{H}_x\mathrm{N}_z)\left(-1 - \frac{4c_\mathrm{N}^2}{3d_\mathrm{HN}^2}\right) + R_2(2\mathrm{H}_x\mathrm{N}_x)\left(1 + \frac{4c_\mathrm{N}^2}{3d_\mathrm{HN}^2}\right)\Bigg\} \quad (8)$$

It is worth reemphasizing that eq 8 is derived under the assumption that $R_{\mathrm{ex},\rho}(2\mathrm{H}_x\mathrm{N}_x)$ is very well approximated by $R_{\mathrm{ex},\rho}(\mathrm{H}_x) + R_{\mathrm{ex},\rho}(\mathrm{N}_x)$. That this is the case under the spin-locking conditions used experimentally is established in the Supporting Information. From eq 8, it is clear that accurate values of both c_N and d_HN are required to obtain meaningful $R_{\mathrm{ex},\rho}$ rates. So long as the "correct" values are used, it is straightforward to show directly from eq 8 that $R_{\mathrm{ex},\rho}$ isolated from the four $R_{1,2}(2\mathrm{H}_\nu\mathrm{N}_\mu)$ rates is independent of molecular tumbling and fast internal dynamics. That is, exchange contributions are completely isolated from ps−ns time-scale motions. However, values of $\Delta\sigma_\mathrm{N}$ are known to vary between residues with $\Delta\sigma_{\mathrm{avg}} = -172$ ppm,[27,35−37] rmsd $(\Delta\sigma_\mathrm{N}) \approx 10$ ppm, leading to some uncertainty in calculated $R_{\mathrm{ex},\rho}(\mathrm{N}_x)$ rates. In general, if a value of c_N is used in eq 8, while the correct value is c, then the error in the calculated $R_{\mathrm{ex},\rho}$ rate, $\Delta R_{\mathrm{ex},\rho}(\mathrm{N}_x) = R_{\mathrm{ex},\rho}(c_\mathrm{N}) - R_{\mathrm{ex},\rho}(c)$, is given by

$$\Delta R_{\mathrm{ex},\rho}(\mathrm{N}_x) = \frac{1}{6}(c_\mathrm{N}^2 - c^2)(3J(\omega_\mathrm{N}) - 4J(0)) \quad (9)$$

so that slightly negative values of $\Delta R_{\mathrm{ex},\rho}(\mathrm{N}_x)$ are derived when the assumed $|\Delta\sigma_\mathrm{N}|$ is larger than the actual value, for example. Thus, $R_{\mathrm{ex},\rho}$ rates may have some dependence on molecular tumbling that reflects the errors in CSA and bond lengths used in the analysis. It is thus conceivable that even in the absence of chemical exchange, nonzero values of $R_{\mathrm{ex},\rho}$ could be obtained (see below). It is worth noting that the same situation occurs, of course, in the measurement of exchange contributions to relaxation from R_1, $R_{1\rho}$, and $^1\mathrm{H}-^{15}\mathrm{N}$ NOE data sets, where uncertainties in constants result in a "mixing" of ps−ns and exchange dynamics as well.

In principle, information about residue-specific variations in $\Delta\sigma_\mathrm{N}$ can be obtained from experiments based on dipole-CSA cross-correlated relaxation,[38] such as those that measure η_{xy}, for example, and subsequently used in analyses that quantify exchange. However, small variations in the angle between the axial component of the CSA tensor and the $^1\mathrm{H}-^{15}\mathrm{N}$ bond vector, and differences in intrinsic dynamics on a per-residue basis, prevent an accurate determination of residue-specific $\Delta\sigma_\mathrm{N}$ from this experiment alone. Rather than attempting to obtain residue-specific $\Delta\sigma_\mathrm{N}$ values and incorporate these into the calculation, we prefer to estimate the uncertainty in $R_{\mathrm{ex},\rho}(\mathrm{N}_x)$ values based on the rmsd of experimentally determined $\Delta\sigma_\mathrm{N}$ and the known dynamics parameters of each protein using eq 9. In what follows, we have used $\Delta\sigma_{\mathrm{avg}} = -172$ ppm, $r_\mathrm{HN} = 1.02$ Å.

As described above, $R_2(2\mathrm{H}_z\mathrm{N}_x)$ and $R_2(2\mathrm{H}_x\mathrm{N}_x)$ relaxation rates used to quantify $R_{\mathrm{ex},\rho}(\mathrm{N}_x)$ are recorded in the presence of a nitrogen spin-lock field that quenches contributions from exchange processes with rate constants smaller than the spin lock field strength.[39] Typically, a 2 kHz $^{15}\mathrm{N}$ spin lock field is applied, so that the resulting exchange contribution calculated from eq 8 is only sensitive to exchange processes faster than $\sim$2000 s^{-1}. More quantitatively, for the case of a system undergoing exchange between two sites, $\mathrm{A} \rightleftharpoons \mathrm{B}$, with forward rate k_A and reverse rate k_B, this contribution is given by[40]

$$R_{\mathrm{ex},\rho}(\mathrm{N}_x) \approx \frac{p_\mathrm{A}p_\mathrm{B}\Delta\omega^2 k_\mathrm{ex}}{\Omega_\mathrm{B}^2 + \omega_\mathrm{SL}^2 + k_\mathrm{ex}^2} \quad (10)$$

where $\Delta\omega = \Omega_\mathrm{B} - \Omega_\mathrm{A}$, with Ω_A and Ω_B the offsets of the $^{15}\mathrm{N}$ resonance frequencies of sites A and B (rad/s) from the nitrogen spin-lock carrier, ω_SL is the field strength of the spin-lock field (rad/s), $k_\mathrm{ex} = k_\mathrm{A} + k_\mathrm{B}$ is the rate of exchange, and the population of the minor state is $p_\mathrm{B} = k_\mathrm{A}/k_\mathrm{ex}$ and $p_\mathrm{A} = 1 - p_\mathrm{B}$. Thus, in concert with eq 8, the four relaxation rates $R_{1,2}(2\mathrm{H}_\nu\mathrm{N}_\mu)$ provide a way to measure contributions from exchange on the order of or faster than $\sim\omega_\mathrm{SL}$. The time-scale of the processes contributing to $R_{\mathrm{ex},\rho}$ can be estimated in a number of ways. For exchange events with frequencies on the order of $\omega_\mathrm{SL}/(2\pi)$, relaxation dispersion experiments are powerful for quantifying the exchange time-scale.[41,42] In cases were both μs and ms processes are present, the exchange parameters isolated from fits of relaxation dispersion profiles can be used to estimate the small contributions to measured $R_{\mathrm{ex},\rho}(\mathrm{N}_x)$ rates from the ms time-scale process (via eq 10) and subtracted from measured $R_{\mathrm{ex},\rho}$ values to "isolate" contributions from μs exchange exclusively, as described later in the text. Further insight can be obtained by measuring $R_{\mathrm{ex},\rho}(\mathrm{N}_x)$ for different offsets of the nitrogen rf-carrier (Ω_B) and/or different nitrogen spin-lock strengths (ω_SL) to extract k_ex in cases where $k_\mathrm{ex} \lesssim 25\,000\ \mathrm{s}^{-1}$.[43] Note that only $R_2(2\mathrm{H}_x\mathrm{N}_x)$ and the $R_2(2\mathrm{H}_z\mathrm{N}_x)$ must be measured as a function of $\{\Omega_\mathrm{B}, \omega_\mathrm{SL}\}$, because $R_1(2\mathrm{H}_z\mathrm{N}_z)$ and $R_2(2\mathrm{H}_x\mathrm{N}_z)$ rates are independent of the nitrogen spin-lock strength and carrier offset. If no variation is observed in $R_{\mathrm{ex},\rho}(\mathrm{N}_x)$, then it follows that $k_\mathrm{ex}^2 \gg \omega_\mathrm{SL}^2 + \Omega_\mathrm{B}^2$, and exchange parameters k_ex, p_b, and $\Delta\omega$ are unfortunately inseparable. If it can be argued that a range of residues are all affected by the same chemical exchange process, as seen previously,[33,44] then the observed $R_{\mathrm{ex},\rho}(\mathrm{N}_x)$, which is proportional to $\Delta\omega^2$, can be used to obtain qualitative information on the structural changes that are involved in the transition. Below we have not attempted to determine the individual exchange parameters, but rather show that accurate $R_{\mathrm{ex},\rho}(\mathrm{N}_x)$ can indeed be obtained.

Validation of the Methodology. In what follows, we consider a pair of proteins, protein L and human ubiquitin, where the exchange contribution $R_{\mathrm{ex},\rho}(\mathrm{N}_x)$ can be quantified both from the measurement of the rates described above (eq 8) and from an independent set of experiments, outlined below. It is known from previous studies that chemical exchange processes for both of these proteins are in the fast-exchange regime, that is, $k_\mathrm{ex} \gg \Delta\omega$. For ubiquitin, residues 23−25, 55, and 70 undergo

(35) Kroenke, C. D.; Rance, M.; Palmer, A. G. *J. Am. Chem. Soc.* **1999**, *121*, 10119–10125.
(36) Hiyama, Y.; Niu, C. H.; Silverton, J. V.; Bavoso, A.; Torchia, D. A. *J. Am. Chem. Soc.* **1988**, *110*, 2378–2383.
(37) Oas, T. G.; Hartzell, C. J.; Dahlquist, F. W.; Drobny, G. P. *J. Am. Chem. Soc.* **1987**, *109*, 5962–5966.
(38) Tjandra, N.; Szabo, A.; Bax, A. *J. Am. Chem. Soc.* **1996**, *118*, 6986–6991.
(39) Palmer, A. G., III; Massi, F. *Chem. Rev.* **2006**, *106*, 1700–1719.
(40) Trott, O.; Palmer, A. G. *J. Magn. Reson.* **2002**, *154*, 157–160.
(41) Palmer, A. G. *Chem. Rev.* **2004**, *104*, 3623–40.
(42) Hansen, D. F.; Vallurupalli, P.; Kay, L. E. *J. Biomol. NMR* **2008**, *41*, 113–20.
(43) Lundström, P.; Akke, M. *J. Biomol. NMR* **2005**, *32*, 163–73.
(44) O'Connell, N. E.; Grey, M. J.; Tang, Y.; Kosuri, P.; Miloushev, V. Z.; Raleigh, D. P.; Palmer, A. G. *J. Biomol. NMR* **2009**, *45*, 85–98.

exchange with a rate constant $k_{ex} \approx 25\,000\ s^{-1}$ at 280 K;[45] thus, $\omega_{SL}^2 + k_{ex}^2 \gg \Omega_B^2$ so that $R_{ex,\rho}(N_x) \propto B_0^2$. Moreover, we have used amide proton $R_{1\rho}$ experiments[43] to probe exchange in protein L. A pair of exchange processes are found, including one affecting the relaxation of residues 4−7 and a second in the vicinity of residues 51−53, with rates of ∼8000 and ∼37 000 s^{-1}, respectively (see Supporting Information), so that $R_{ex,\rho} \propto B_0^2$ in this case as well.

Because the fast exchange condition applies for both ubiquitin and protein L (although not in general for all proteins, see below), $R_{ex,\rho}(N_x)$ can be measured using a second approach for these proteins distinct from the one described above, in which the exchange contribution is extracted from ^{15}N R_1, $R_{1\rho}$ relaxation rates and steady-state $^1H-^{15}N$ NOE values measured at multiple magnetic fields,[23] using the relation $R_{ex,\rho}(N_x) \propto B_0^2$ (see below). The rotating frame relaxation rate is given by

$$R_{1\rho}(N_x) = R_1(N_z)\cos^2\theta + R_2(N_x)\sin^2\theta \qquad (11)$$

where $\tan\theta = \omega_{SL}/\Omega$ and $\Omega = p_A\Omega_A + p_B\Omega_B$ is the offset of the exchange averaged resonance position from the carrier (rad/s). In eq 11,

$$R_2(N_x) = \left(\frac{d_{HN}^2}{8} + \frac{c^2}{6}\right)(4J(0) + 3J(\omega_N)) + 1.349d_{HN}^2J(0.87\omega_H) + R_{ex,\rho}(N_x) + \vartheta_N \qquad (12)$$

where the high-frequency spectral density terms, $J(\omega_H + \omega_N)$, $J(\omega_H)$, and $J(\omega_H - \omega_N)$, have been combined into a term proportional to $J(0.87\omega_H)$, as described above. A spectral density mapping of R_1, $R_{1\rho}$, and $^1H-^{15}N$ NOE values measured at static magnetic fields of 11.7 and 18.8 T (six measurables) into five discrete values of the power spectral density function $\{J(0), J(\omega_{N,11.7T}), J(\omega_{N,18.8T}), J(0.87\omega_{H,11.7T}), J(0.87\omega_{H,18.8T})\}$ and an additional parameter that accounts for the exchange, ξ, where $R_{ex,\rho}(N_x) = \xi B_0^2$, is performed that then allows the determination of $R_{ex,\rho}(N_x)$ from the relaxation data. Figure 1 illustrates the comparison of $R_{ex,\rho}(N_x)$ values derived from the four $R_{1,2}(2H_\nu N_\mu)$ relaxation rates measured at 18.8 T (eq 8) and from spectral density mapping of R_1, $R_{1\rho}$, and $^1H-^{15}N$ NOE data recorded at 11.7 and 18.8 T for both ubiquitin (Figure 1a) and protein L (Figure 1b). Overall, there is a very good correlation between $R_{ex,\rho}(N_x)$ rates derived by the two different methods, cross-validating the present approach. A similar plot is shown in the Supporting Information where $R_{ex,\rho}(N_x)$ rates derived from $R_{1,2}(2H_\nu N_\mu)$ values measured at 11.7 T are compared to the corresponding R_{ex} rates derived from spectral density mapping of R_1, $R_{1\rho}$, and $^1H-^{15}N$ NOE data. Remarkably, even very small $R_{ex,\rho}(N_x)$ contributions are determined accurately, and the agreement between the two methods is high once again. What then is the advantage of measuring $\{R_{1,2}(2H_\nu N_\mu)\}$? First, the four $R_{1,2}(2H_\nu N_\mu)$ values need be acquired at only one static magnetic field strength, in this case 18.8 T (Figure 1, or 11.7 T as in the Supporting Information), obviating the need for data at two or more fields that are necessary in the spectral density mapping approach. This is a considerable benefit because it avoids errors associated with different spectrometer usage (temperature differences, slight differences in ω_{SL} values between the measurements at different fields) that can become important for the quantification of small exchange contributions. In addition, assumptions about the dependence of $R_{ex,\rho}(N_x)$ on B_0 are not needed (here we have shown that the quadratic dependence is justified, but this will not be the case in general[23]). One might argue that an appropriate spin-lock field strength, ω_{SL}, can be chosen in a conventional $R_{1\rho}$ experiment to ensure that $R_{1\rho}$ is always proportional to B_0^2 (see eq 10). However, because in practice chemical shifts of the excited state are likely not to be available, strong spin-lock fields (3 kHz) must be used to ensure that $R_{ex,\rho}$ follows a quadratic B_0 dependence. Of course, the application of such strong fields would exacerbate the difficulties in ensuring identical sample temperatures for experiments recorded at the multiple magnetic fields, a requirement for the $R_{1\rho}$ analysis. Moreover, very strong fields lead to efficient quenching of the exchange effect that is to be measured in the first place. The approach described here where four $R_{1,2}(2H_\nu N_\mu)$ rates are measured at a single field avoids these issues.

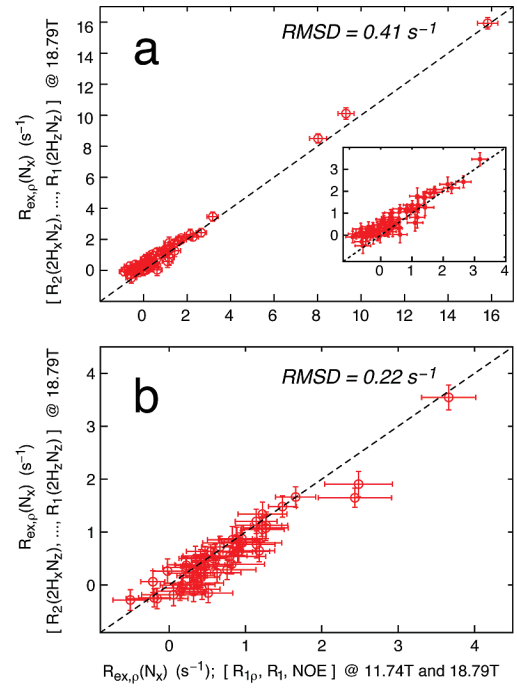

Figure 1. Exchange contributions $R_{ex,\rho}(N_x)$ obtained from measurement of residue-specific $R_2(2H_xN_z)$, $R_2(2H_zN_x)$, $R_2(2H_xN_x)$, and $R_1(2H_zN_z)$ relaxation rates at a magnetic field strength of 18.8 T (*y*-axis) agree with the corresponding values isolated from ^{15}N R_1, ^{15}N $R_{1\rho}$, and $^1H-^{15}N$ NOE measurements at two static magnetic fields (11.7 and 18.8 T) for U-^2H,^{15}N-labeled human ubiquitin (a) and U-^2H,^{15}N-labeled protein L (b), 278 K. A ^{15}N spin-lock field strength of 2 kHz was used for all experiments. The dashed lines correspond to $y = x$, and the rmsd is calculated as $\sqrt{(\Sigma(x_i - y_i)^2/N)}$. The inset in (a) shows an expansion of the region corresponding to small $R_{ex,\rho}(N_x)$ rates. A similar plot is shown in the Supporting Information where $R_{ex,\rho}(N_x)$ was obtained from $R_2(2H_xN_z)$, $R_2(2H_zN_x)$, $R_2(2H_xN_x)$, and $R_1(2H_zN_z)$ relaxation rates measured at a magnetic field strength of 11.7 T.

Studies of Ubiquitin and Protein L Establish Significant Microsecond Fluctuations Even in These Thermostable Proteins. Residue-specific $R_{ex,\rho}(N_x)$ rates, obtained from measured $R_{1,2}(2H_\nu N_\mu)$ values, are shown for ubiquitin (at 278 K, Figure 2a; and 298 K, Figure 2c) and for protein L (278 K, Figure 2b). The error introduced due to the uncertainty in the magnitude of the CSA, δ_{CSA} (site-specific variation in $\Delta\sigma_N$ of ±10 ppm[27,35−37]), is combined with each residue-specific experimental error in $R_{ex,\rho}(N_x)$, δ_{Exp} (red vertical bars), to generate the total error $\delta_{Total} = \sqrt{(\delta_{Exp}^2 + \delta_{CSA}^2)}$, shown as light blue error bars in Figure 2. From eq 9, it is clear that δ_{CSA} depends on the rotational correlation time. Herein, we have assumed that δ_{CSA} corresponds to an error in the assumed $\Delta\sigma_N$ value of 10 ppm so that $\delta_{CSA} \approx 0.4\ s^{-1}$ for ubiquitin at 278 K (Figure 2a), $\approx 0.5\ s^{-1}$ for protein L at 278 K (Figure 2b), and

(45) Massi, F.; Grey, M. J.; Palmer, A. G. *Protein Sci.* **2005**, *14*, 735–742.

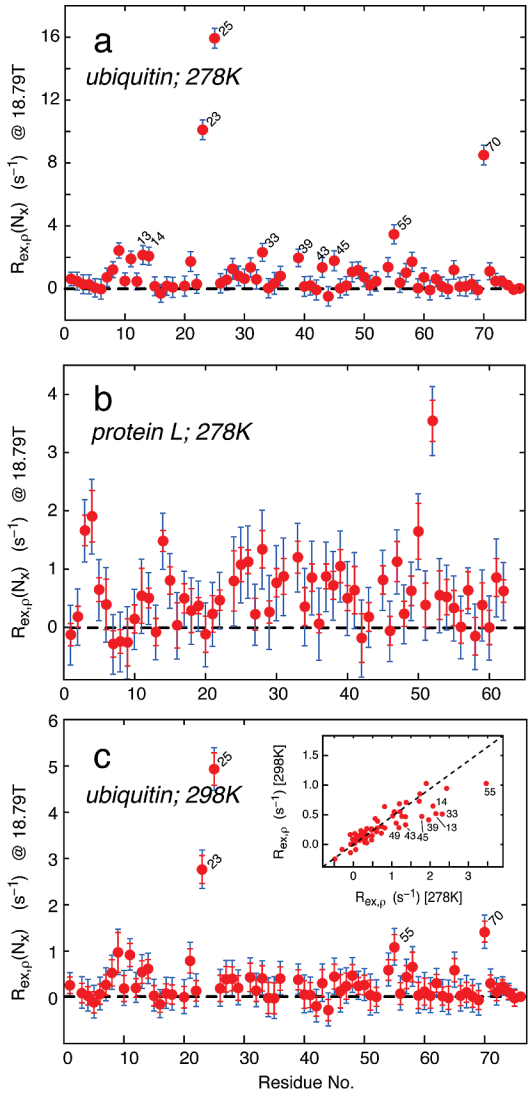

Figure 2. Residue-specific microsecond chemical exchange contributions, $R_{ex,\rho}(N_x)$, derived from the four relaxation rates $R_2(2H_xN_z)$, $R_2(2H_zN_x)$, $R_2(2H_xN_x)$, and $R_1(2H_zN_z)$ for (a) human ubiquitin at 278 K, (b) protein L at 278 K, and (c) ubiquitin at 298 K. The inset in (c) is a comparison of $R_{ex,\rho}(N_x)$ derived at 278 K versus $R_{ex,\rho}(N_x)$ derived at 298 K for ubiquitin. An ^{15}N spin-lock field strength of 2 kHz was used to monitor the $R_2(2H_zN_x)$ and $R_2(2H_xN_x)$ rates. The red error bars correspond to the experimental error in the determination of $R_{ex,\rho}(N_x)$, while the blue error bars include both experimental errors and errors introduced by the uncertainty in $\Delta\sigma_N$ ($\pm$10 ppm), as described in the text.

≈ 0.25 s^{-1} for ubiquitin at 298 K (Figure 2c). Only those residues for which $R_{ex,\rho}(N_x) - \delta_{Total} > 0$ are considered to show exchange.

Several residues of human ubiquitin have previously been identified to exhibit chemical exchange (e.g., 23−25, 43, 45, 55, and 70), and clearly these residues show large $R_{ex,\rho}(N_x)$ contributions in Figure 2a. However, many more residues show significant exchange contributions, such as 9−14. Similarly, many significant $R_{ex,\rho}(N_x)$ values are observed for protein L (Figure 2b), in particular for residues in the α helix region that includes amino acids 25−42. Thus, for both of these proteins, microsecond chemical exchange seems to be localized to α helical and loop regions and is certainly much more extensive than observed before.

It is worth noting that the derived exchange contributions cannot be due to simple exchange of amide protons with solvent, because such contributions will rigorously cancel in the linear combination of eqs 7 and 8. Neither can protein aggregation be a factor because $R_{ex,\rho}(N_x)$ is independent of overall protein concentration over the 3−4-fold concentration range examined for both ubiquitin and protein L (see Supporting Information). Large site-specific variations of $\Delta\sigma_N$ suggested earlier[46−48] could explain some of the chemical exchange contributions observed in Figure 2; however, to account for all of the residues not previously identified as undergoing exchange,[45] an average value of $\langle\Delta\sigma\rangle = -179$ ppm (ubiquitin) and $\langle\Delta\sigma\rangle = -186$ ppm (protein L) must be used, at variance with previous solid-state[36,37] and solution-state NMR studies.[27] Further evidence that the elevated $R_{ex,\rho}(N_x)$ rates are interpreted correctly in terms of microsecond exchange comes from a temperature-dependent study of ubiquitin where $R_{ex,\rho}(N_x)$ is measured at 298 and 278 K. At the higher temperature, the exchange contributions are attenuated as shown in a comparison of Figure 2a and c, likely reflecting an increase in k_{ex} (eq 10). That exchange must be present can be "visualized" in an alternate manner, as shown in the inset to Figure 2c. Recall that the derived $R_{ex,\rho}(N_x)$ rates from eq 8 are nonzero when the value of $\Delta\sigma_N$ used differs from the actual residue-specific CSA value, even in the absence of chemical exchange. That is, $R_{ex,\rho}^{measured} = R_{ex,\rho}^{correct} + 1/6(c_N^2 - c^2)(3J(\omega_N) - 4J(0))$, eq 9. Moreover, assuming only very small changes in internal dynamics with temperature, it follows that

$$\left\langle \frac{[4J(0) - 3J(\omega_N)]_{298K}}{[4J(0) - 3J(\omega_N)]_{278K}} \right\rangle = 0.47 \pm 0.02 \qquad (13)$$

so that $R_{ex,\rho}^{measured,298} = 0.47R_{ex,\rho}^{measured,278}$ in the absence of exchange and when $c_N^2 \neq c^2$. Those residues for which $R_{ex,298K}/R_{ex,278K}$ values significantly differ from 0.47 (Figure 2c, inset) must experience microsecond exchange, and site-specific variation of $\Delta\sigma_N$ cannot explain the observed deviations. Indeed, $R_{ex,\rho}(N_x)_{298} < 0.47R_{ex,\rho}(N_x)_{278}$ for many of the ubiquitin residues with statistically significant $R_{ex,\rho}(N_x)$ (Figure 2a,c, numbered residues). It is worth noting that while $R_{ex,\rho}(N_x)_{298} < 0.47R_{ex,\rho}(N_x)_{278}$ implies exchange, residues for which $R_{ex,\rho}(N_x)_{298} = 0.47R_{ex,\rho}(N_x)_{278}$ may also undergo exchange because contributions from exchange and overall tumbling could scale approximately the same way with temperature.

Color-coded values of $R_{ex,\rho}(N_x)$ calculated from measured $R_{1,2}(2H_\nu N_\mu)$ rates using eq 8 are plotted on the structures of ubiquitin (Figure 3) and protein L (Figure 4). It is clear that residues with microsecond chemical exchange include those in α-helices, loops, and to some extent on the strands that define the "rim" of β sheets. By contrast, very limited μs exchange is present for amide nitrogens located in the core of β sheets. Of interest, residues 9−14 in ubiquitin, which are shown here to have elevated $R_{ex,\rho}(N_x)$ values, have been identified in a previous study based on residual dipolar couplings to have enhanced dynamics[2] and play a role in a conformational selection process, which facilitates the binding of this protein to its many targets.[51] This study makes clear that even thermo-stable proteins that

(46) Fushman, D.; Tjandra, N.; Cowburn, D. *J. Am. Chem. Soc.* **1998**, *120*, 10947–10952.
(47) Hall, J. B.; Fushman, D. *J. Am. Chem. Soc.* **2006**, *128*, 7855–7870.
(48) Burton, R. A.; Tjandra, N. *J. Biomol. NMR* **2006**, *35*, 249–259.
(49) Cornilescu, G.; Marquardt, J. L.; Ottiger, M.; Bax, A. *J. Am. Chem. Soc.* **1998**, *120*, 6836–6837.
(50) O'Neill, J. W.; Kim, D. E.; Baker, D.; Zhang, K. Y. J. *Acta Crystallogr., Sect. D: Biol. Crystallogr.* **2001**, *57*, 480–487.
(51) Hicke, L.; Schubert, H. L.; Hill, C. P. *Nat. Rev. Mol. Cell Biol.* **2005**, *6*, 610–21.

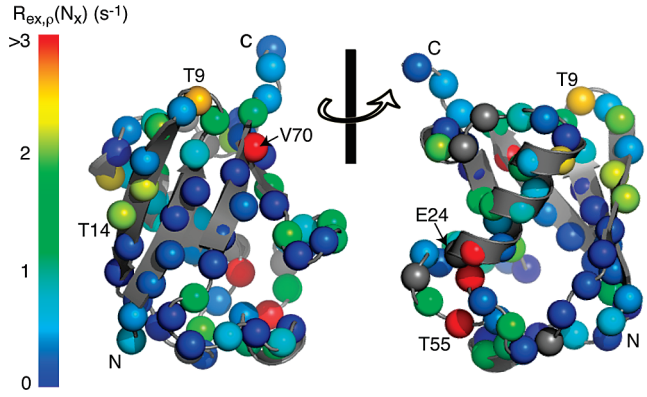

Figure 3. Microsecond chemical exchange contributions for human ubiquitin depicted on the 3D structure (pdb 1D3Z).[49] The rims of the β sheet, the α helix, and in particular the loop regions show significant $R_{ex,\rho}(N_x)$ contributions due to microsecond molecular fluctuations, which are absent from the protein core. The orientation in (a) is similar to that presented previously in a study focusing on dynamics based on residual dipolar couplings,[2] while (b) is a view from a different angle. Residues with large $R_{ex,\rho}(N_x)$ are indicated on the structure. No data are available for residues depicted with gray color.

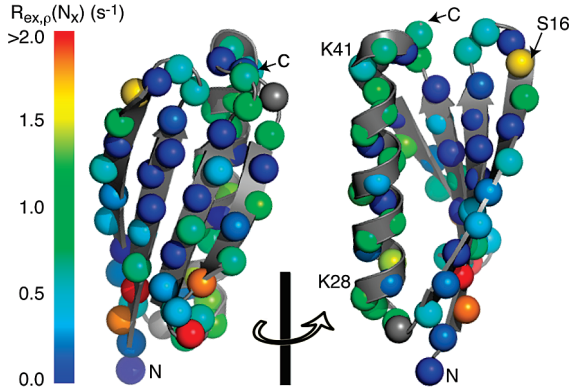

Figure 4. Microsecond chemical exchange contributions for protein L shown on the 3D structure (pdb 1HZ6).[50] The loop regions and the α helix between K28 and K41 show significant $R_{ex,\rho}(N_x)$ rates, which are absent in the core of the β sheet. No data are available for residues depicted with gray color.

have been thought previously to be very rigid, such as ubiquitin and protein L, can have rather pervasive μs dynamics. Indeed, such a result must have been anticipated by the early pioneers in the biomolecular NMR field,[52−54] who showed that aromatic groups in proteins can undergo a wide range of motions on very different time-scales that must involve significant structural rearrangements.

Microsecond Time-Scale Motions in a Histone−Chaperone Complex. Many molecular complexes are dynamic over a wide range of time-scales, and it is often of interest to separate the different motional processes according to their frequencies. One such complex involves the histone chaperone Chz1 that transports and delivers the variant histone H2A.Z to the nucleosomal remodeling complex,[20] which, in turn, inserts H2A.Z into nucleosomes to alter levels of gene expression in eukaryotic cells. The binding kinetics and in particular the stability and dynamics of the Chz1:H2A.Z-H2B complex may be key for understanding both the delivery process and the function of this chaperone. Previous studies of the association/dissociation reaction:[21]

$$\text{H2A.Z-H2B:Chz1} \underset{k_{off}}{\overset{k_{on}}{\rightleftharpoons}} \text{H2A.Z-H2B} + \text{Chz1} \qquad (14)$$

have established that $k_{off} = 22 \pm 2$ s^{-1}, $k_{on} = 10^8 \pm 10^7$ M^{-1} s^{-1}, and $K_D = 0.22 \pm 0.02$ μM, 35 °C. These values were obtained by CPMG relaxation dispersion measurements that are sensitive to the millisecond time-scale association/dissociation that occurs when a near 1:1 mixture of chaperone and histone is present. In addition to this process, there are significant "fast" local fluctuations over a range extending from 100 ps to 2 ns,[55] overall rotation of the complex (∼12 ns), and, as we show below, extensive μs dynamics. The pico−nanosecond fluctuations cause line narrowing of NMR signals, with both the millisecond and the microsecond time-scale processes leading to line broadening. The entanglement of these various processes makes their separation challenging.

As described above, the key to the separation of μs from ms exchange events lies in the use of kHz spin-lock fields that suppress contributions from the ms time-scale process. For ^{15}N experiments that monitor the fate of Chz1 during the binding reaction of eq 14, the exchange rate is given by $k_{ex} = k_{on} \times$ [H2A.Z-H2B] + k_{off}, and previous studies have shown that for (total) concentrations of Chz1 and H2A.Z-H2B ≈ 1 mM employed presently, $k_{ex} \approx k_{on}$[H2A.Z-H2B] = 1500 s^{-1} at 35 °C. Thus, contributions to $R_{ex,\rho}(N_x)$ from ligand association/dissociation, $R_{ex,ass}$, will be largely quenched by the 2 kHz ^{15}N spin-lock field ($\omega_{SL,N}$) used to record $R_2(2H_yN_x)$ rates, because $k_{ex} < \omega_{SL,N}$. More quantitatively,

$$R_{ex,ass} \approx \frac{p_{Chz1}\Delta\omega^2_{ass/diss}k_{ass}}{\Omega^2_{Chz1} + \omega^2_{SL} + k^2_{ass}} \qquad (15)$$

where $\Delta\omega_{ass/diss} = \Omega_{Chz1} - \Omega_{Chz1:H2A.Z-H2B}$, with Ω_{Chz1} and $\Omega_{Chz1:H2A.Z-H2B}$ the offsets of ^{15}N resonance frequencies of probes in free and bound Chz1 from the spin-lock carrier (rad/s), k_{ass} is the pseudo first-order rate constant for the reaction, k_{on}[H2A.Z-H2B], and $p_{Chz1} \ll 1$ is the population of free Chz1. Values of $R_{ex,ass}$ were calculated for all residues of Chz1 using measured chemical shift changes $|\Delta\omega_{CPMG}|$, $p_{Chz1} = 1.5\%$, and $k_{ass} = 1500$ s^{-1} derived earlier from relaxation dispersions experiments.[21] For all residues of Chz1, $R_{ex,ass} < 3.5$ s^{-1}, with $R_{ex,ass} < 1.1$ s^{-1} for 96% of the ^{15}N sites. Thus, even though it is a reasonable approximation to assume that millisecond processes are quenched effectively by the spin-lock, the "pure" contribution from microsecond dynamics can be calculated as $R_{ex,\mu s} = R_{ex,\rho}(N_x) - R_{ex,ass}$.

Large microsecond exchange contributions are observed for residues 94−115 of Chz1, encompassing the CHZ recognition motif that plays an important role in stabilizing the Chz1:H2A.Z-H2B ternary complex,[55] Figure 5. By contrast, $R_{ex,\mu s}$ values are much smaller for the N- and C-terminal helices. Although the time-scale(s) of the microsecond motions cannot be calculated directly from the $R_{ex,\mu s}$ rates, estimates can be made. Microsecond processes must be of the same order of or faster than the nitrogen spin-lock frequency (2000 Hz) used in the $R_{ex,\rho}(N_x)$ measurements to avoid quenching by

(52) Wuthrich, K.; Wagner, G. *Trends Biochem. Sci.* **1978**, *3*, 227–230.
(53) Campbell, I. D.; Dobson, C. M.; Williams, R. J. P. *Proc. R. Soc. London, Ser. B* **1975**, *189*, 503–509.
(54) Snyder, G. H.; Rowan, R.; Sykes, B. D. *Biochemistry* **1976**, *15*, 2275–2283.
(55) Zhou, Z.; Feng, H.; Hansen, D. F.; Kato, H.; Luk, E.; Freedberg, D. I.; Kay, L. E.; Wu, C.; Bai, Y. *Nat. Struct. Mol. Biol.* **2008**, *15*, 868–9.

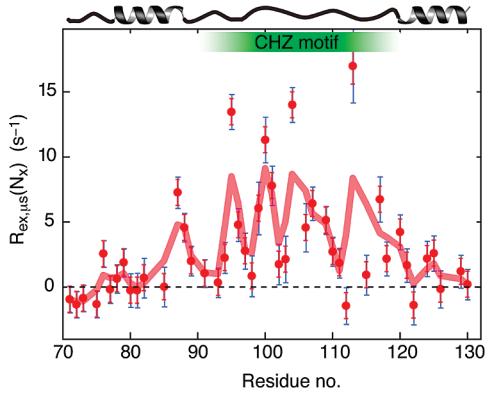

Figure 5. Exchange contributions to ^{15}N transverse relaxation rates, $R_{ex,\rho}(N_x)$, of Chz1 in the ternary Chz1:H2A.Z-H2B complex from dynamic processes with time-scales faster than ~0.5 ms. The secondary structure elements are shown on the top of the plot. The thick pale red line is a "running average" calculated as $R_{ex,avg}(i) = 0.25R_{ex}(i-1) + 0.5R_{ex}(i) + 0.25R_{ex}(i+1)$. Large $R_{ex,\rho}(N_x)$ values are primarily observed for residues 94−115 (the CHZ motif), whereas the N-cap and C-cap helices only show small contributions from microsecond dynamics. The red error bars correspond to the experimental error, whereas the blue error bars are calculated to take into account both the variability of CSA values (from −182 to −162 ppm[27,35−37]) and the experimental error (see text and legend of Figure 2).

the spin-lock field (see above), but sufficiently slow so that self-quenching does not occur (note that $R_{ex,\rho}$ becomes small for large k_{ex}, eq 10). Assuming two-site exchange with a limiting scenario of $p_B = 50\%$ and $\Delta\omega_N = 10$ ppm, $\omega_{SL} = 2$ kHz, then k_{ex} must be less than 4×10^5 s^{-1} to account for the $R_{ex,\mu s}$ values observed in Figure 5. Thus, our experiments establish that the CHZ motif of Chz1 bound to histones H2A.Z-H2B is dynamic on a microsecond time-scale, ranging between 2.5 and 500 μs. Such motion may well affect the stability of the complex and may play a role in regulating dissociation of chaperone that is strongly anchored to H2A.Z-H2B by a large interaction surface and strong electrostatic attractive forces.

In summary, we have presented a new approach for quantifying microsecond time-scale dynamics in proteins from chemical exchange contributions, $R_{ex,\mu s}$, to amide nitrogen transverse relaxation rates. The method is based on the measurement of four relaxation rates that can be combined in a straightforward manner to isolate exchange contributions on a per-residue basis. Notably, the influence of millisecond ($k_{ex} < 2000$ s^{-1}) motions is effectively eliminated by recording individual relaxation rates in the presence of a nitrogen spin-lock field of approximately 2 kHz. Perhaps surprisingly, rather extensive microsecond time-scale dynamics have been detected in both human ubiquitin and protein L, two molecules that are thermo-stable and that are likely more rigid than many other proteins. Such motions are located exclusively in α helices, loops, and on the rim of β sheets, with the β sheet core much less dynamic. The results from the present work suggest, therefore, that microsecond dynamics are likely to be more pervasive in proteins than previously thought. Finally, it has also been shown that microsecond motions can be separated from other chemical exchange processes, as demonstrated in the context of a histone−chaperone complex. Relaxation data measured at only a single static magnetic field are required. The described method will provide a very useful addition to a growing body of backbone spin-relaxation measurements that quantify dynamics over a wide range of time-scales and that provide insight into the relation between motion and protein function.

Material and Methods

Sample Preparation. U-[^{15}N,^{2}H] human ubiquitin was expressed with a cleavable His-tag and purified by standard methods.[56] A pair of protein samples with concentrations of 2.2 and 0.7 mM were prepared using a 20 mM Na_3PO_4, 10 mM NaCl, 0.03% NaN_3, 90%/10% H_2O/D_2O, pH 5.5 buffer. U-[^{15}N,^{2}H]-protein L was produced as described previously.[57] Two protein L samples were obtained with protein concentrations of 2.7 and 0.5 mM in 50 mM Na_3PO_4, 20 μM EDTA, 0.05% NaN_3, 90%/10% H_2O/D_2O, pH 6.0 buffer. An approximate 1:1 mixture of U-[^{15}N,^{2}H] Chz1 (~1 mM) and U-[^{15}N,^{2}H] single-chain H2A.Z-H2B (~1 mM) was prepared as described previously[55] in a buffer consisting of 25 mM MES, 200 mM NaCl, 1 mM EDTA, pH 6.0, and 10% D_2O.

NMR Spectroscopy. The four relaxation rates $R_2(2H_xN_z)$, $R_2(2H_zN_x)$, $R_2(2H_xN_x)$, and $R_1(2H_zN_z)$ were derived for human ubiquitin ((278 K; 0.7 mM), (278 K; 2.2 mM), and (298 K; 2.2 mM)), for protein L ((278 K; 0.5 mM) and (278 K; 2.3 mM),) and for Chz1 in the Chz1:H2A.Z-H2B ternary complex (308 K) at a static magnetic field strength of 18.8 T (800 MHz proton frequency), using pulse schemes for measuring the rotating frame relaxation rates, $R_{1\rho}(2H'_zN_z)$, $R_{1\rho}(2H_zN'_z)$, $R_{1\rho^2}(2H'_zN'_z)$, and $R_1(2H_zN_z)$, that have been published previously.[23] Briefly, the rotating frame antiphase relaxation rate, $R_{1\rho}(2H'_zN_z)$, was measured with ^{1}H magnetization spin-locked[58] along an effective field that is given by the vector-sum of the spin-lock field ($\omega_{SL,H} \approx 13$ kHz, along x) and the offset of the ^{1}H nucleus from the ^{1}H radio frequency (rf) carrier (Ω_H, along z), $\vec{\omega}_{eff,H} = \vec{\omega}_{SL,H} + \vec{\Omega}_H$. The proton carrier was placed at 9.5 ppm as suggested previously.[23] It follows directly that $2H'_zN_z = \sin(\theta_H)2H_xN_z + \cos(\theta_H)2H_zN_z$, where $\tan\theta_H = \omega_{SL,H}/\Omega_H$, and consequently it can be shown that

$$R_{1\rho}(2H'_zN_z) = R_2(2H_xN_z)\sin^2\theta_H + R_1(2H_zN_z)\cos^2\theta_H \quad (16)$$

Similarly, $R_{1\rho}(2H_zN'_z)$ was measured with the ^{15}N magnetization spin-locked along an effective nitrogen field so that

$$R_{1\rho}(2H_zN'_z) = R_2(2H_zN_x)\sin^2\theta_N + R_1(2H_zN_z)\cos^2\theta_N \quad (17)$$

where $\tan\theta_N = \omega_{SL,N}/\Omega_N$, $\omega_{SL,N}$ is the strength (rad/s) of the ^{15}N spin-lock field, and Ω_N is the offset (rad/s) of the ^{15}N nucleus from the ^{15}N radio frequency carrier placed at 119 ppm. Finally, the "double-rotating frame" rate, $R_{1\rho^2}(2H'_zN'_z)$, was measured with ^{1}H and ^{15}N magnetization spin-locked along their respective fields so that

$$\begin{aligned} R_{1\rho^2}(2H'_zN'_z) = {} & R_2(2H_xN_x)\sin^2\theta_H\sin^2\theta_N + \\ & R_2(2H_xN_z)\sin^2\theta_H\cos^2\theta_N + R_2(2H_zN_x)\cos^2\theta_H\sin^2\theta_N + \\ & R_1(2H_zN_z)\cos^2\theta_H\cos^2\theta_N \end{aligned} \quad (18)$$

The transverse relaxation rates $R_2(2H_xN_z)$, $R_2(2H_zN_x)$, and $R_2(2H_xN_x)$ were derived from the four measured relaxation rates $R_{1\rho}(2H'_zN_z)$, $R_{1\rho}(2H_zN'_z)$, $R_{1\rho^2}(2H'_zN'_z)$, and $R_1(2H_zN_z)$ via eqs 16−18 and used in subsequent analyses.

The relaxation rates $R_{1,2}(2H_\nu N_\mu)$ were measured with delays of 2.5, 5.3, 8.3, 11.5, 15.1, 19.2, 23.7, 28.8, 35 ms (ubiquitin and protein L) and 2, 3.8, 5.9, 8, 10.4, 12.8, 15.5, 18.4, 21.5 ms for the histone−chaperone complex. ^{1}H and ^{15}N continuous wave (CW) spin-lock field strengths varied between 11.5 and 13.7 kHz for ^{1}H

(56) Distefano, D. L.; Wand, A. J. *Biochemistry* **1987**, *26*, 7272–7281.
(57) Scalley, M. L.; Yi, Q.; Gu, H. D.; McCormack, A.; Yates, J. R.; Baker, D. *Biochemistry* **1997**, *36*, 3373–3382.
(58) Hansen, D. F.; Kay, L. E. *J. Biomol. NMR* **2007**, *37*, 245–255.

(depending on the sample) and were very close to 1.9 kHz for ^{15}N. Nitrogen R_1 and $R_{1\rho}$ relaxation rates along with steady-state ^{1}H$-^{15}$N NOE values[59] were obtained for the backbone amides of ubiquitin (298 and 278 K) and protein L (278 K) at static magnetic field strengths of 11.7 and 18.8 T. Relaxation delays of 0.01, 0.1, 0.21, 0.34, 0.49, 0.67, 0.67, and 0.9 s were used for the R_1 measurements, while the $R_{1\rho}$ rates were quantified from experiments recorded with delays of 2, 9.5, 20, 32, 60, 78, and 100 ms. In all cases, the ^{15}N field strength applied during the spin-lock period in the $R_{1\rho}$ experiments was very close to 1.9 kHz, with fine-power adjustments to ensure that identical spin-lock powers were used for a given sample at both static magnetic fields. ^{1}H$-^{15}$N NOE values were quantified from two spectra, with and without proton presaturation. The spectrum with presaturation was recorded with a prescan delay of 9 s followed by 6 s of proton saturation, while the spectrum without proton presaturation was recorded with a 15 s prescan delay.

Data Processing. Data sets were processed with the NMRPipe program[60] and analyzed with UCSF Sparky.[61] Signal intensities were determined using the program FuDA (flemming@pound.med.utoronto.ca; http://pound.med.utoronto.ca/software) by fitting a mixed Gaussian/Lorentzian line-shape to each correlation and assuming a common line-shape for a given cross-peak within a relaxation series (i.e., line-shape and peak positions are independent of relaxation delay). All relaxation rates were determined by fitting a single exponential decay function, $I(T_{relax}) = A \exp(-RT_{relax})$, to the measured intensity versus T_{relax} profile. Microsecond chemical exchange contributions, $R_{ex,\rho}$, were calculated using eq 8. Uncertainties in relaxation rates were obtained from the covariance matrix method[62] and propagated with a Monte Carlo procedure.

Acknowledgment. We would like to thank Professors Silke Wiesner (Max Planck Institute for Developmental Biology, Tübingen, Germany) and Voula Kanelis (University of Toronto, Canada) for preparing the human ubiquitin and protein L samples, respectively. This work was supported by a grant from the Canadian Institutes of Health Research (CIHR). D.F.H. acknowledges a postdoctoral fellowship from CIHR. L.E.K. is the recipient of a Canada Research Chair in Biochemistry.

Supporting Information Available: Figure S1: Exchange in protein L is fast on the NMR chemical shift time-scale. Figure S2: Same correlation as in Figure 1 but with $R_{ex,\rho}(N_x)$ values obtained from $R_2(2H_xN_z)$, $R_2(2H_zN_x)$, $R_2(2H_xN_x)$, and $R_1(2H_zN_z)$ relaxation rates measured at a magnetic field strength of 11.7 T. Figure S3: To an excellent approximation, $R_{ex}(H_x) + R_{ex}(N_x) = R_{ex}(H_xN_x)$ using the spin-lock experiments described in this Article. Figures S4 and S5: No aggregation for either ubiquitin or protein L in the concentration ranges used in the present study. Figure S6: Contributions from external protons are negligibly small for ubiquitin. Derivation of eq 7. This material is available free of charge via the Internet at http://pubs.acs.org.

JA906842S

(59) Farrow, N. A.; Muhandiram, R.; Singer, A. U.; Pascal, S. M.; Kay, C. M.; Gish, G.; Shoelson, S. E.; Pawson, T.; Forman-Kay, J. D.; Kay, L. E. *Biochemistry* **1994**, *33*, 5984–6003.
(60) Delaglio, F.; Grzesiek, S.; Vuister, G. W.; Zhu, G.; Pfeifer, J.; Bax, A. *J. Biomol. NMR* **1995**, *6*, 277–293.
(61) Kneller, D. G.; Kuntz, I. D. *J. Cell. Biochem.* **1993**, 254–254.
(62) Press, W. H.; Flannery, B. P.; Teukolsky, S. A.; Vetterling, W. T. *Numerical Recipes in C*; Cambridge University Press: Cambridge, 1988.